Microchimica Acta (2020) 187:455
https://doi.org/10.1007/s00604-020-04425-1

ORIGINAL PAPER

An electrochemiluminescence biosensor for p53 antibody based on Zn-MOF/GO nanocomposite and Ag^+-DNA amplification

Yu-ping Wei[1] · Yi-wen Zhang[1] · Jing-Shuai Chen[1] · Chang-jie Mao[1] · Bao-Kang Jin[1]

Received: 31 March 2020 / Accepted: 30 June 2020

Abstract

An ultrasensitive electrochemiluminescence biosensor was established based on the Zn-MOF/GO nanocomposite. Ag(I)-embedded DNA complexes were used as a signal amplification reagent. In this work, 5,10,15,20-tetrakis(4-carboxyphenyl)porphyrin (TCPP) and Zn^{2+} were integrated into a porphyrin paddlewheel framework (Zn-MOF) by a hydrothermal method. The synthesized Zn-MOF material has electrochemiluminescence property, and the luminescence intensity is improved after being composited with graphene oxide (GO). Based on the composite material, we constructed an ultrasensitive ECL biosensor for the p53 antibody detection. The composite material acted as an admirable substrate and then loaded plenty of p53 antigens to recognize the target (p53 antibody) accurately. Because of the bridging effect of streptavidin and biotin-conjugated goat anti-rabbit IgG (bio-ab2), the rich-C DNA with positive correlation with the target was modified on the electrode and then captured the co-reactant accelerator Ag^+ to amplify the signal. Therefore, the ECL biosensor response increases with increasing p53 antibody concentration. In the range 0.1 fg/mL–0.01 ng/mL, the response signal of the biosensor has a good linear relationship with the p53 antibody concentration. The detection limit is 0.03 fg/mL ($S/N = 3$). Impressively, the biosensor not only featured high sensitivity, good stability, and excellent specificity for the detection of p53 antibody, but also provides a new way for early detection of cancer.

Keywords Electrochemiluminescence biosensor · Metal-organic framework · Porphyrin · Co-reactant accelerator · P53 antibody

Introduction

Cancer is a type of difficult-to-cure human disease and has an extremely high fatality rate [1]. For cancer patients, the sooner the disease is discovered, the more likely it is that the disease is effectively controlled. Early detection of cancer is critical. p53 antibody is a kind of the autoantibody and can be discovered in human serum after the mutations of the p53 gene [2–6]. p53 antibody was observed in the serum of different cancerous person such as breast, liver, ovarian, and lung cancer [7–9]. Hence, p53 antibody has been recognized as a significant cancer marker and the highly sensitive detection of p53 antibody is important in the early diagnosis of cancer. The detection of p53 antibody is generally carried out by immunoprecipitation [10], western blotting [11], ELISA [12], and electrochemical immunosensing [13]. However, the disadvantages of complicated procedures, high cost, and low sensitivity limit the widespread application of these methods.

Electrochemiluminescence technology is a combined method of electrochemistry and spectroscopy. By integrating the advantages of both technologies, the ECL biosensor has become a powerful tool (high sensitivity, low background, ease of control, and simple equipment) in immunosensing and environmental and food monitoring [14–22]. The traditional ECL materials include luminol and its analogues, fluorescent dyes, noble-metal nanoclusters, quantum dots, and some carbon materials [23]. Metal-organic framework (MOF) nanomaterials have emerged in recent years [24].

Electronic supplementary material The online version of this article (https://doi.org/10.1007/s00604-020-04425-1) contains supplementary material, which is available to authorized users.

✉ Jing-Shuai Chen
cjshuai@126.com

✉ Chang-jie Mao
maochangjie@sina.com

[1] Key Laboratory of Structure and Functional Regulation of Hybrid Materials (Ministry of Education), Anhui Province Key Laboratory of Chemistry for Inorganic/Organic Hybrid Functionalized Materials, School of Chemistry & Chemical Engineering, Anhui University, Hefei, Anhui 230601, People's Republic of China

MOFs are famous for their chemical tunability, structural flexibility, ultrahigh porosity, easy modification, and huge equivalent. They are widely used in gas separation and storage, molecular magnets, catalysis, photovoltaic materials, and other applications [25–29]. However, MOFs have only lately emerged in ECL applications. Our research group previously combined CdSe QDs and MIL-101 in one step by a hydrothermal method and achieved high ECL intensity and an ultrasensitive immunosensor for carcinoembryonic antigen [28]. Researchers have attempted to introduce $Ru(bpy)_3^{2+}$ into the structure of MOFs to form ECL materials [30, 31]. However, 5,10,15,20-tetrakis(4-carboxyphenyl)porphyrin as a novel cathodic ECL luminescent reagent [32] and a highly coordinating macrocyclic compound was hardly ever studied in construct MOF materials as an ECL luminescent reagent. Here, we integrated TCPP and Zn^{2+} into a porphyrin paddlewheel framework and built an ECL biosensor on the Zn-MOF.

In this work, the synthesized zinc tetrakis(4-carboxyphenyl)-porphyrin complexes (Zn-MOF) was a stronger ECL emitter compared with TCPP. After combining with graphene oxide, the ECL intensity was effectively amplified because the electron transfer rate was accelerated by the graphene oxide. Then, the compounds were successfully modified onto a cleaned glassy carbon electrode to establish an excellent working electrode. Thanks to the specific bonding between the biological materials, an ultrasensitive biosensor has gradually been established. In the final modification step, the DNA backbone was modified with silver ions at a concentration positively correlated with the p53 antibody. The ECL response signal increased with increasing p53 antibody concentration because of the amplification of Ag^+ as a co-reactant accelerator [33]. Therefore, a highly sensitive ECL biosensor was built successfully for p53 antibody detection.

Experimental section

Materials and reagents

Anisole, salicylic acid, N, N-dimethylformamide (DMF), and 4,4′-biphenyldicarboxylic acid (BPDC) were obtained from Shanghai Macklin Biochemical Co., Ltd. (Shanghai China). Pyrrole and methyl p-formylbenzoate were bought from Aladdin Reagent Co., Ltd. (Shanghai, China). Methanol, graphite powder, potassium permanganate, zinc nitrate hexahydrate, tetrahydrofuran, potassium hydroxide, and benzoic acid were purchased from Shanghai Reagent Co. Ltd. (Shanghai, China). Glutaraldehyde (50% aqueous solution) was provided by Shanghai Sangon Biological Engineering Technology Co. Ltd. (Shanghai, China). Bovine serum albumin (BSA), p53 antigen, p53 antibody, streptavidin, rich-C biotin-DNA, biotin-conjugated goat anti-rabbit IgG (bio-ab2), and prostate-specific antigen (PSA) were acquired from Sigma-Aldrich Co. Ltd. (Shanghai, China). Urokinase-type plasminogen activator (u-PA) and carcinoembryonic (CEA) were provided by Beijing Biosynthesis Biotechnology Co. Ltd. (Beijing, China). Mucin 1 (MUC1) was provided by Shanghai Apeptide Co., Ltd. (Shanghai, China). All of the above reagents were analytically pure and without further purification. Phosphate-buffered saline (PBS; pH = 7.4, 10 mM) consisted of 1.76 mM KH_2PO_4, 10.15 mM Na_2HPO_4, 136.89 mM NaCl, and 2.67 mM KCl. Ultrapure water (18 MΩ cm) was used throughout this work.

Rich-C biotin-DNA (bio-DNA): biotin-AAA AAA CCT CCT CCT CCT TTT CCT CCT CCT CC.

Apparatus

A scanning electron microscope (SEM; REGULUS8230, HITACHI, Japan). X-ray polycrystalline diffractometer (XRD; Smartlab 9kW, Rigoku, Japan), Fourier transform infrared spectrometer (FTIR; NEXUS-870, Nicolet Instrument Co., USA), X-ray photoelectron spectroscopy (XPS; ESCALAB 250, Thermo Ltd., USA) were used. The cyclic voltammetry (CV) and ECL were performed on the CHI-660D electrochemical workstation (Shanghai Chenhua Instrument, China) and MPI-E electrochemiluminescence analyzer (Xi′an Remax Co. Ltd., China) respectively. During the measurements, Ag/AgCl electrode, Pt wire electrode, and the modified glassy carbon electrode (GCE) were used as a reference electrode, auxiliary electrode, and working electrode respectively. The voltage of photomultiplier was set at 800 V. Electrochemical impedance spectroscopy (EIS) was carried out on an Autolab electrochemical analyzer (EcoChemie Co., Netherlands) in 5 mM Fe $(CN)_6^{3-/4-}$ and 0.1 M of KCl.

Preparation of the Zn-MOF and Zn-MOF/GO

The preparation of the Zn-MOF and Zn-MOF/GO was placed in the Electronic Supporting Material (ESM).

Preparation of the biosensor

The glassy carbon electrode was polished with alumina powder and cleaned with deionized water and ethanol for further use. Ten microliters of Zn-MOF/GO and 5 μL of chitosan solution (0.1 wt%, aqueous solution) were dropped respectively onto the GCE electrode and dried at room temperature. Then, the amino group of chitosan was activated by introducing 10 μL of 5% glutaraldehyde solution on the surface of the electrode. Ten microliters of p53 antigen solution (distributed in 10 mM PBS buffer) was modified on the electrode and incubated at 4 °C for 12 h. To block the nonspecific binding sites, 10 μL of BSA (2 wt% 10 mM PBS) was introduced onto the electrode. After rinsing, 10 μL of p53 antibody (1 pg/mL 10 mM PBS, the concentration of the p53 antibody is variable in

other testing processes) was incubated at 30 °C on the surface of the electrode for 1 h. The p53 antibody was expected to bond with the p53 antigen. Then, 10 μL of biotin-conjugated goat anti-rabbit IgG was added and incubated for 1 h. After rinsing gently, 10 μL of streptavidin solution was introduced to the electrode. After incubation at 37 °C for 30 min, the modified electrode was further incubated with bio-DNA solution. Finally, the electrode was incubated with $AgNO_3$ solution (0.1 M) for 30 min at 37 °C to form the Ag(I)-embedded DNA complexes (Ag^+-DNA), and then the electrode was stored at 4 °C as a backup. The modified electrode was rinsed gently with deionized water after each step and dried with N_2. The assembly of the proposed ECL biosensor is shown in Scheme 1.

ECL measurement procedure

After the construction of the biosensor, the electrode was immersed in 0.12 M $K_2S_2O_8$ solution (10 mM PBS pH 7.4) to obtain the ECL signal and the photomultiplier tube (PMT) high voltage was 800 V.

Result and discussion

Characterization of Zn-MOF and Zn-MOF/GO

The morphology of Zn-MOF and Zn-MOF/GO was characterized by SEM. Zn-MOF particles exhibited an independent regular quadrangular prism structure (Fig. 1a and b). The morphology of Zn-MOF/GO is shown in Fig. 1c and d. It was obvious that thin layer GO coated the Zn-MOF particles. The crystal structures of the Zn-MOF and Zn-MOF/GO were confirmed by XRD and are shown in Fig. 1e. The Zn-MOF (curve a) displayed four peaks at 5.8, 7.09, 8.4, and 17.6 degrees which were assigned to the (100), (110), (002), and (004) crystallographic planes [34]. Compared with Zn-MOF, there was no significant change in the diffraction peaks of Zn-MOF/GO (curve b). Therefore, the crystallinity of the Zn-MOF had not been disrupted. The FTIR spectroscopy results are shown in Fig. 1f. Curve a represents the FTIR spectrum of TCPP. The vibrational peaks at 3318 cm^{-1} and 966.47 cm^{-1} represented the stretching vibration and in-plane bending vibration of N–H, respectively. The stretching vibration and deformation vibration of O–H in carboxyl were located at 2700–2500 cm^{-1}. The C=O stretching vibration in carboxyl functional groups was observed at 1692 cm^{-1}. Compared with the spectra of Zn-MOF (curve b), the bending vibration of N–H at 966.47 cm^{-1} was replaced by the stretching of Zn–N at 1001.08 cm^{-1}. This result proved the successful synthesis of Zn-MOF. After combination with graphene oxide (curve c), the C=O peak of GO shifted from 1734 to 1666 cm^{-1}. This change confirmed that the interaction between GO and Zn-MOF was hydrogen bonding and π-π packing [35-37].

The chemical structures of Zn-MOF are shown by XPS (Fig. 2). Figure 2 indicates that the elements of Zn, C, O, and N are existing in Zn-MOF. As shown in Figure 2, the Zn 2p XPS spectra had two characteristic peaks at 1045.5 and 1022.4 eV, which could be attributed to Zn 2p1/2 and Zn 2p3/2, respectively. The XPS signal of C 1s at 284.8, 286.6, and 288.8 eV (Fig. 2c) were attributed to the C–C,

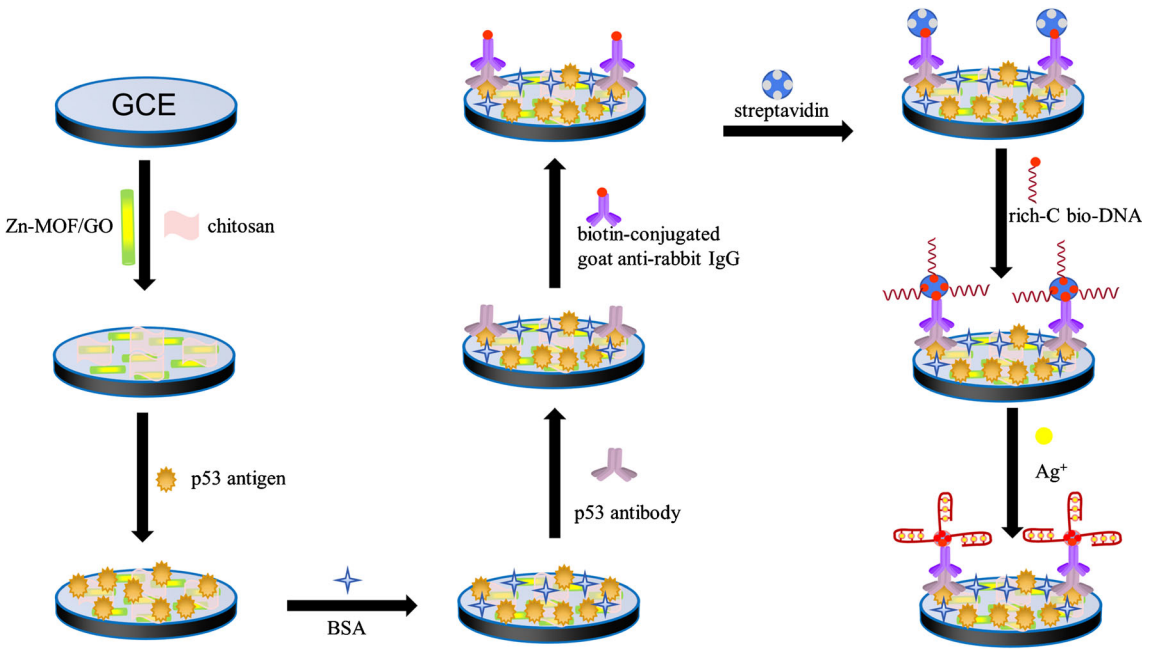

Scheme 1 A schematic diagram of the ECL biosensor buildings process

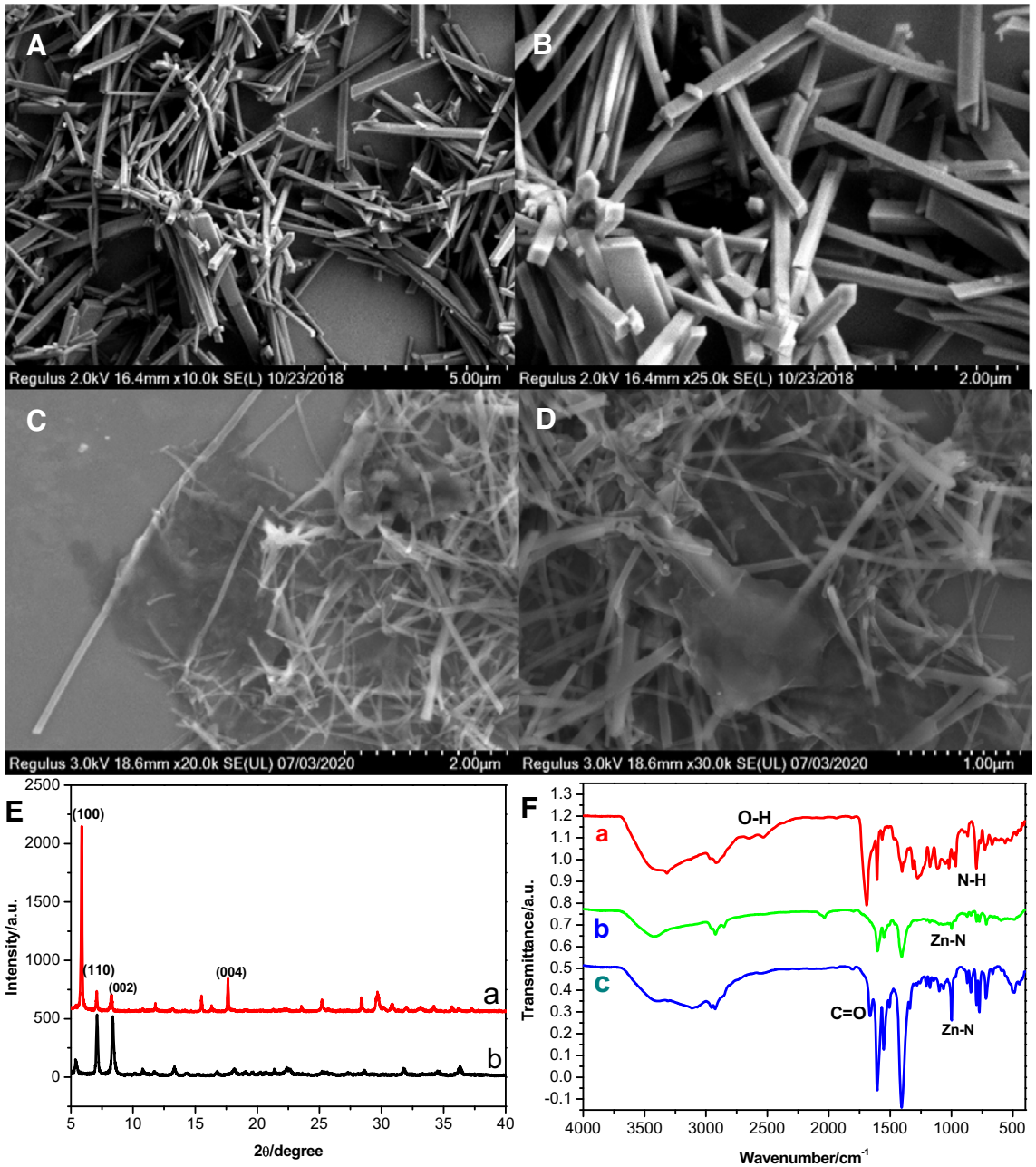

Fig. 1 SEM images of **a**, **b** Zn-MOF and **c**, **d** Zn-MOF/GO. **e** P-XRD of (a) Zn-MOF and (b) Zn-MOF/GO. **f** FTIR spectra of (a) TCPP, (b) Zn-MOF, and (c) Zn-MOF/GO

C–O, and C=O bonds in the Zn-MOF. The N 1s peaks (Fig. 2d) are located at 401.2 and 398.5 eV, and the N 1s peaks in TCPP are located at 400.1 eV and 397.95 eV (Fig. 2f). The difference between Zn-MOF and TCPP was caused by coordination with zinc. The XPS signal of O 1s (Fig. 2e) was split into three peaks at 532.4 eV (C–O), 531.2 eV (C=O), and 530.1 eV (Zn–O) [38, 39].

The ECL potential curve and CV responses obtained in 0.1 M $K_2S_2O_8$ solution are shown in Fig. 3a and b. Compared with TCPP (curve a), the ECL intensity of Zn-MOF (curve b) was doubled. The void structure in the Zn-MOF increased the effective reaction area; therefore, the ECL intensity had been amplified. After compositing with graphene oxide (curve c), the ECL intensity increased further. This was caused by the excellent conductivity of GO. In Fig. 3b, the reduction current of bare GCE increased with the potential at − 0.708 V. The reduction peaks of TCPP/GCE existed at − 0.818 V and − 1.232 V. The reduction peaks of Zn-MOF were appeared at − 1.041 and − 1.326 V. Compared with Zn-MOF, the intensity of Zn-MOF/GO was higher and this phenomenon means that GO promoted the speed of electron transfer. In Fig. 3c,

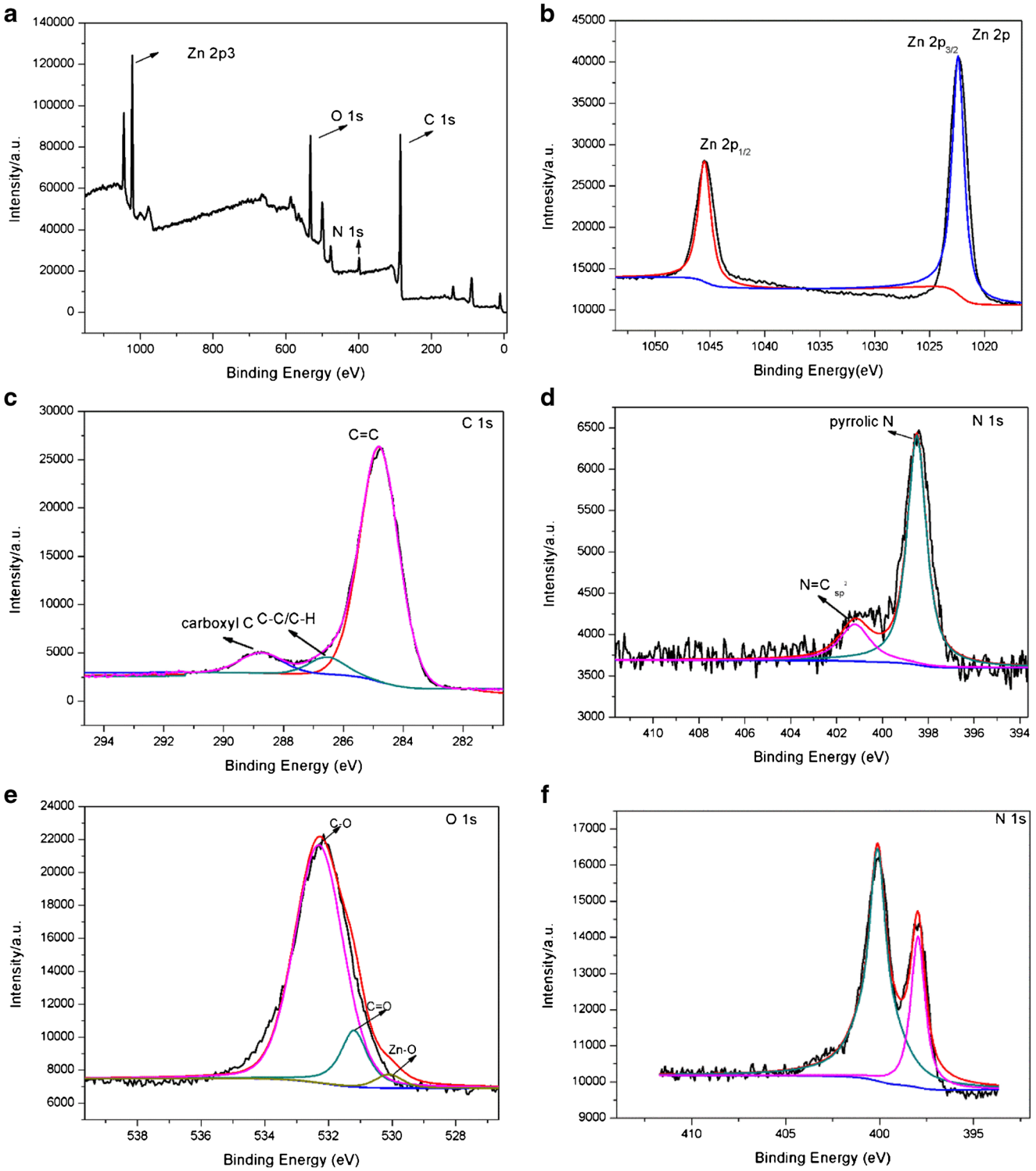

Fig. 2 XPS analysis of the full region of Zn-MOF (**a**) and different elements Zn 2p (**b**), C 1s (**c**), N 1s (**d**), O 1s (**f**), and N 1s (**e**) in TCPP

the ECL stability of Zn-MOF/GO was studied, and the modified electrode was continuously scanned for 15 cycles at − 0.2–1.8 V, and the scan rate was 0.1 V/s. The relative standard deviation (RSD) was 1.3%, suggesting good stability of the complex.

Feasibility of the biosensor

EIS and CV were employed to verify the fabrication of the biosensor. As shown in Figure S2A, the EIS Nyquist plot contained a semicircle portion, which corresponded

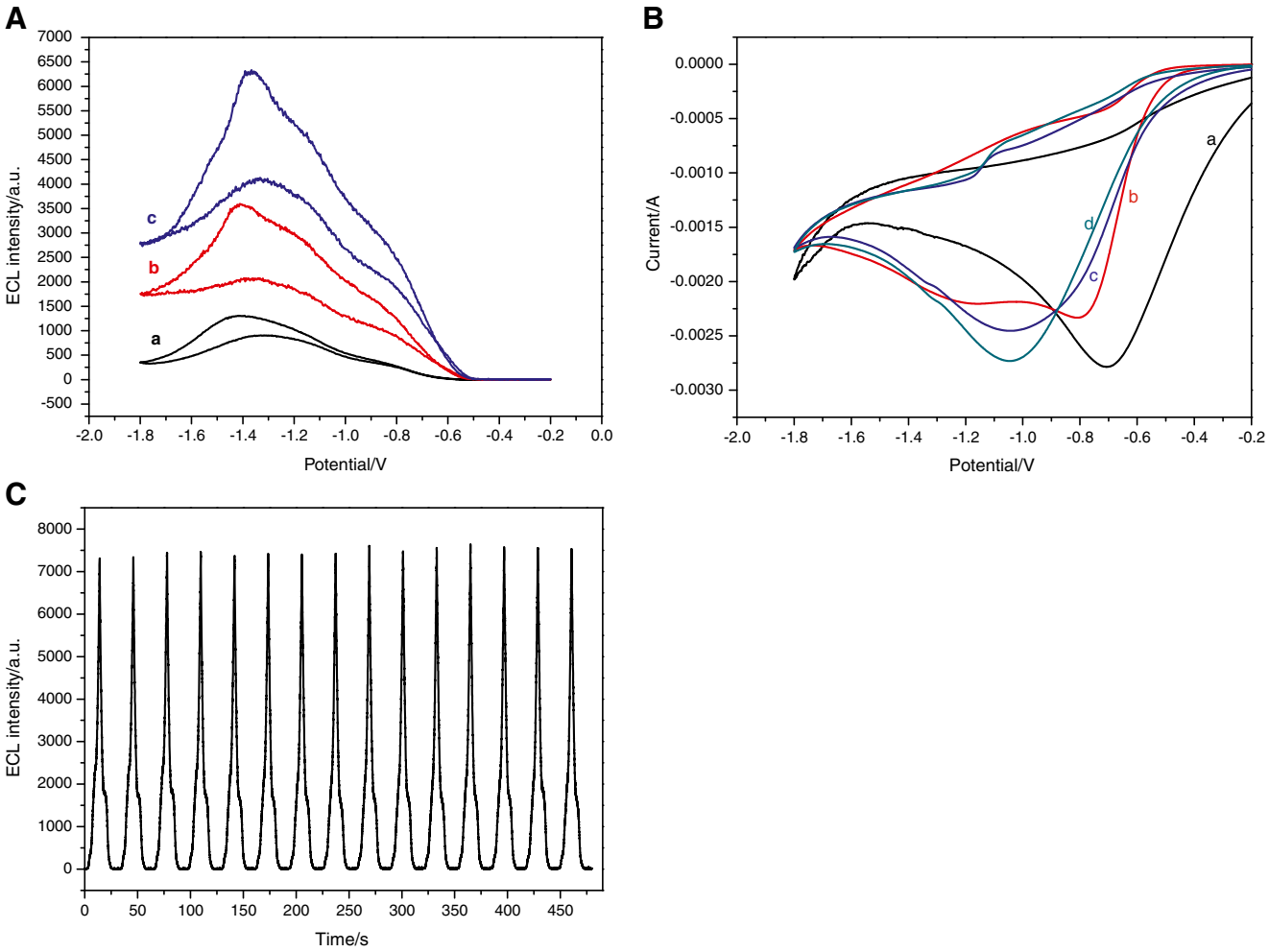

Fig. 3 **a** ECL intensity-potential curves of TCPP (a), Zn-MOF (b), and Zn-MOF/GO (c). **b** CV curves of GCE (a), TCPP/GCE (b), Zn-MOF/GCE (c), and Zn-MOF/GO/GCE (d) in $K_2S_2O_8$ solution. **c** The stability of Zn-MOF/GO

to the higher frequency region and reflected the electron transfer restricted process (Ret). The bare electrode (curve a) showed a tiny semicircle in the EIS Nyquist plot (Ret = 74.09 Ω), which indicated the good conductivity of the electrode. After the modification of Zn-MOF/GO on the electrode (curve b), the impedance increased to 226.3 Ω. The biomacromolecule prevented the transformation of electrons on the electrode. Hence, after p53 antigen, BSA, p53 antibody, bio-ab2, streptavidin, and biotin-DNA successfully assembled on the electrode, the impedance increased continuously and significantly (p53 antigen, Ret = 1064 Ω, curve c; BSA, Ret = 3361 Ω, curve d; p53 antibody, Ret = 5428 Ω, curve e; biotin-conjugated goat anti-rabbit IgG, Ret = 7401 Ω, curve f; streptavidin Ret = 9939 Ω, curve g; and biotin-DNA, Ret = 11,210 Ω, curve h). When the Ag^+ was conjugated with rich-C DNA, the resistance value decreased to 6416 Ω (curve i), because the positively charged Ag^+ could decrease the negative charges of DNA, reducing the resistance between the $[Fe(CN)_6]^{3-/4-}$ and the electrode surface.

The CV responses of different modified electrodes are shown in Figure S2B. A pair of well-defined current peaks of $[Fe(CN)_6]^{3-/4-}$ were obtained for the bare electrode (curve a). Corresponding to the impedance, the CV response decreased gradually after the electrode was modified by degrees (curves b–h). As shown in curve i, the Ag^+-modified electrode had a higher current peak, due to the reduced resistance of $[Fe(CN)_6]^{3-/4-}$ on the electrode surface.

Optimization of the experimental conditions

The optimization of the experimental conditions was placed in ESM.

Performance of the biosensor for p53 antibody

The p53 antibody was detected under the optimal conditions. As observed in Fig. 4a, the ECL intensity clearly increased with the p53 antibody concentration from 0.1 fg/mL to 0.01 ng/mL. In Fig. 4b, the ECL response was proportional

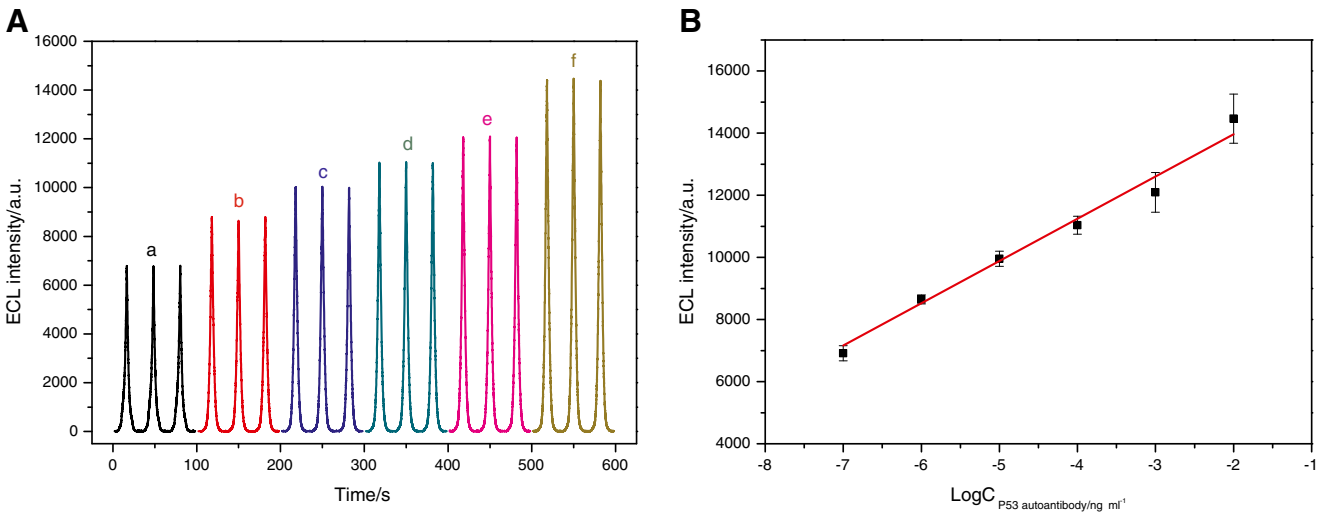

Fig. 4 **a** ECL response and **b** calibration curve for different p53 antibody levels (a: 0.1 fg/mL, b: 1 fg/mL, c: 0.01 pg/mL, d: 0.1 pg/mL, e: 1 pg/mL, f: 0.01 ng/mL)

to the logarithm of the p53 antibody concentration from 0.1 fg/mL to 0.01 ng/mL. The regression equation of the biosensor was $I = 1360.23$ lg C + 16,685.89 (correlation coefficient 0.989), and the detection limit was 0.03 fg/mL ($S/N = 3$). Compared with previous studies (Table S1), our biosensor had a lower detection limit. These results indicated that this biosensor had excellent sensitivity to the target.

Selectivity and stability of this biosensor

Selectivity is an important index for an excellent biosensor. The selectivity of this proposed biosensor was examined under the same optimal conditions by challenging this strategy against other proteins (shown in Fig. 5), including 1 pg/mL u-PA, PSA, CEA, and MUC1. The ECL intensity was not significantly magnified compared with 0.01 pg/mL p53 antibody. For the mixed samples (containing 1 pg/mL u-PA, PSA, CEA, and MUC1 and 0.01 pg/mL p53 antibody), the biosensor response was similar to that obtained for 0.01 pg/mL p53 antibody. These results indicated that the proposed biosensor could selectively and specifically detect p53 antibodies. The stability of the developed biosensor was tested by storing the electrode at 4 °C for 2 weeks, and the ECL response changed slightly (89% of its initial intensity).

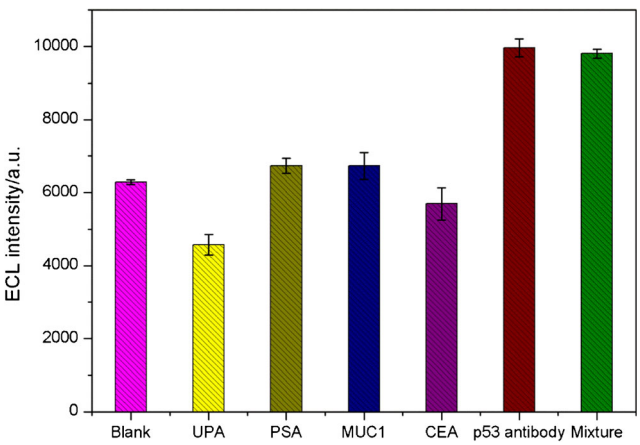

Fig. 5 Selectivity of the ECL biosensor with different targets from left to right: blank sample (1 pg/mL u-PA, 1 pg/mL PSA, 1 pg/mL MUC1, 1 pg/mL CEA, and 0.01 pg/mL p53 antibody) and the mixed sample (containing 1 pg/mL u-PA, 1 pg/mL PSA, 1 pg/mL MUC1, 1 pg/mL CEA, and 0.01 pg/mL p53 antibody)

Detection of the real sample

The biosensor was applied in the detection of the real sample. The application potential of the proposed biosensor could be illustrated by the detection of the real samples. The p53 antibody standard added to healthy human serum was detected. Firstly, human serum was diluted 10 times with 10 mM PBS buffer. Then, p53 antibody was diluted by human serum to different concentrations and detected using the biosensor. As shown in Table S2, the recovery levels were 107%, 92%, and 102.3%, respectively. Therefore, the ECL biosensor has great potential for the sensitive and accurate detection of p53 antibody in real samples.

Conclusion

We found an excellent ECL emitter (Zn-MOF/GO nanocomposite material) and built an ultrasensitive and high selectivity ECL biosensor based on the nanocomposite material. In this biosensor, Ag^{+}-DNA was used as a co-reactant accelerator to amplify the ECL signal. In the presence of the target p53 antibody, the bio-ab2 and streptavidin could be modified on

the electrode to bind the rich-C DNA. The Ag+ were captured by rich-C DNA via C-C mismatches to form stable Ag(I)-embedded DNA complexes and then enhance the ECL intensity further. Hence, the increased ECL signal associated with the concentration of p53 antibody. The ECL biosensor not only had excellent performance for p53 antibody detection, but also had feasibility for the detection of other biomolecules through changing the specific recognition protein. However, this biosensor has several disadvantages; for example, it is time-consuming for a single set of samples and requires more reagents. Hence, we will devote ourselves to the research of simpler and more time-saving biosensors.

Funding information This work was supported by the National Natural Science Foundation of China (21976001), Natural Science Foundation of Anhui Province (1808085QB53), and open fund for Discipline Construction of Institute of Physical Science and Information Technology.

Compliance with ethical standards The protocol of this study was approved by the medical ethics committee of The First Affiliated Hospital of Anhui Medical University. Human Serum Samples were also provided by The First Affiliated Hospital of Anhui Medical University. The blood samples (2 mL) of the participants were collected after informed written consent was provided by the subjects.

Conflict of interest The authors declare that they have no competing of interests.

References

1. Torre LA, Bray F, Siegel RL, Ferlay J, Lortet-Tieulent J, Jemal A (2015) Global cancer statistics, 2012. CA Cancer J Clin 65:87–108
2. Yeo JC, Park JY, Bae WJ, Lee YS, Kim BH (2009) Label-free electrochemical detection of the p53 core domain protein on its antibody immobilized electrode. Anal Chem 81:4770–4777
3. Vogelstein B, Lane D, Levine AJ (2000) Surfing the p53 network. Nature 408:307–310
4. Yang LL, Tao YZ, Yue GY, Li RB, Qiu B, Guo LH, Lin ZY, Yang H (2016) Highly selective and sensitive electrochemiluminescence biosensor for p53 DNA sequence based on nicking endonuclease assisted target recycling and hyperbranched rolling circle amplification. Anal Chem 88:5097–5103
5. Lane DP (1992) Cancer. p53, guardian of the genome. Nature 358: 15–16
6. Schlichtholz B (1992) The immune response to p53 in breast cancer patients is directed against immunodominant epitopes unrelated to the mutational hot spot. Cancer Res 52:6380–6384
7. Winter SF (1992) Development of antibodies against p53 in lung cancer patients appears to be dependent on the type of p53 mutation. Cancer Res 52:4168–4174
8. Atta MM, El-Masry SA, Abdel-Hameed M, Baiomy HA, Ramadan NE (2008) Value of serum anti-p53 antibodies as a prognostic factor in Egyptian patients with hepatocellular carcinoma. Clin Biochem 41:1131–1139
9. Anderson KS, Wong J, Vitonis A, Crum CP, Sluss PM, Labaer J, Cramer D (2010) P53 autoantibodies as potential detection and prognostic biomarkers in serous ovarian cancer. Cancer Epidemiol Biomarkers Prev 19:859–868
10. Lubin R, Zalcman G, Bouchet L, Tredanel J, Legros Y, Cazals D, Hirsch A, Soussi T (1995) Serum p53 antibodies as early markers of lung cancer. Nat Med 1:701–702
11. Mudenda B, Green JA, Green B, Jenkins JR, Robertson L, Tarunina M, Leinster SJ, The relationship between serum p53 autoantibodies and characteristics of human breast cancer (1994) Br J Cancer 69: 1115–1119
12. Portefaix J, Fanutti C, Granier C, Crapez E, Perham R, Grenier J, Pau B, Del Rio M (2002) Detection of anti-p53 antibodies by ELISA using p53 synthetic or phage-displayed peptides. J Immunol Methods 259:65–75
13. Elshafey R, Siaj M, Tavares AC (2016) Au nanoparticle decorated graphene nanosheets for electrochemical immunosensing of p53 antibodies for cancer prognosis. Analyst 141:2733–2740
14. Ge JJ, Zhao Y, Gao XS, Li HK, Jie GF (2019) Versatile electrochemiluminescence and photoelectrochemical detection of glutathione using Mn^{2+} substitute target by DNA walker-induced allosteric switch and signal amplification. Anal Chem 91:14117–14124
15. Ge JJ, Zhao Y, Li CL, Jie GF (2019) Versatile electrochemiluminescence and electrochemical "on−off" assays of methyltransferases and aflatoxin B1 based on a novel multifunctional DNA nanotube. Anal Chem 91:3546–3554
16. Wang J, Zhuo Y, Zhou Y, Wang HJ, Yuan R, Chai YQ (2016) Ceria doped zinc oxide nanoflowers enhanced luminol-based electrochemiluminescence immunosensor for amyloid-β detection. ACS Appl Mater Interfaces 8:12968–12975
17. Ke H, Sha H, Wang Y, Guo W, Zhang X, Wang Z, Huang C, Jia N (2017) Electrochemiluminecence resonance energy transfer system between GNRs and Ru(bpy)32+: application in magnetic aptasensor for β-amyloid. Biosens Bioelectron 100:266–273
18. Wen W, Yan X, Zhu C, Du D, Lin Y (2017) Recent advances in electrochemical immunosensors. Anal Chem 89:138–156
19. Hu GB, Xiong CY, Liang WB, Zeng XS, Xu HL, Yang Y, Yao LY, Yuan R, Xiao DR (2018) Highly stable mesoporous luminescence-functionalized MOF with excellent electrochemiluminescence property for ultrasensitive immunosensor construction. ACS Appl Mater Interfaces 10:15913–15919
20. Cho KG, Lee JI, Lee S, Hong KY, Kang MS, Lee KH (2020) Light-emitting devices based on electrochemiluminescence gels. Adv Funct Mater 2020:1907936
21. Babamiri B, Bahari D, Salimi A (2020) Highly sensitive bioaffinity electrochemiluminescence sensors: recent advances and future directions. Biosens Bioelectron 142:111530
22. Valenti G, Rampazzo E, Kesarkar S, Genovese D, Fiorani A, Zanut A, Palomba F, Marcaccio M, Paolucci F, Prodi L (2018) Electrogenerated chemiluminescence from metal complexes-based nanoparticles for highly sensitive sensors applications. Coord Chem Rev 367:65–81
23. Hou LL, Zhou BB (2019) Electrochemiluminescent biosensors for the detection of microRNAs: a review. Int J Electrochem Sci 14: 2489–2508
24. Abednatanzi S, Derakhshandeh PG, Depauw H, Coudert FX, Vrielinck H, Voort PVD, Leus K (2019) Mixed-metal metal–organic frameworks. Chem Soc Rev 48:2497–2658
25. Lin X, Jia JH, Zhao XB, Thomas KM, Blake AJ, Walker GS, Champness NR (2010) High H_2 adsorption by coordination-framework materials. Angew Chem Int Ed Eng 118:7518–7524
26. Li JR, Kuppler RJ, Zhou HC (2009) Selective gas adsorption and separation in metal–organic frameworks. Chem Soc Rev 38:1477–1504

27. Liu Q, Yang Y, Liu XP, Wei YP, Mao CJ, Chen JS, Niu HL, Song JM, Zhang SY, Jin BK, Jiang M (2016) A facile in situ synthesis of MIL-101-CdSe nanocomposites for ultrasensitive electrochemiluminescence detection of carcinoembryonic antigen. Sensors Actuators B Chem 242:1073–1078
28. Murray LJ, Dinca M, Long JR (2009) Hydrogen storage in metal–organic frameworks. Chem Soc Rev 38:1294–1314
29. Dong X, Zhao G, Liu L, Li X, Wei Q, Cao W (2018) Ultrasensitive competitive method-based electrochemiluminescence immunosensor for diethylstilbestrol detection based on $Ru(bpy)_3^{2+}$, as luminophor encapsulated in metal–organic frameworks UiO-67. Biosens Bioelectron 110:201–206
30. Zhao GH, Wang YG, Li XJ, Yue Q, Dong X, Du B, Cao W, Wei Q (2019) Dual-quenching electrochemiluminescence strategy based on three-dimensional metal−organic frameworks for ultrasensitive detection of amyloid-β. Anal Chem 91:1989–1996
31. Luo D, Huang B, Wang L, Idris AM, Wang SX, Lu XQ (2015) Cathodic electrochemiluminescence of meso-tetra(4-carboxyphenyl) porphyrin/potassium peroxydisulfate system in aqueous media. Electrochim Acta 151:42–49
32. Zhao YM, Ling J, Li SG, Li M, Liu AR, Liu SQ (2018) Synthesis of porphyrin-based two-dimensional metal–organic framework nanodisk with small size and few layers. J Mater Chem A 6:2828–2833
33. Ge JJ, Li CL, Zhao Y, Yu XJ, Jie GF (2019) Versatile "on–off" biosensing of thrombin and miRNA based on Ag(I) ion-enhanced or Ag nanocluster-quenched electrochemiluminescence coupled with hybridization chain reaction amplification. Chem Commun 55:7350–7353
34. Ye L, Gao Y, Cao SY, Chen H, Yao YN, Hou JG, Sun LC (2018) Assembly of highly efficient photocatalytic CO_2 conversion systems with ultrathin two-dimensional metal–organic framework nanosheets. Appl Catal B Environ 227:54–60
35. Jahan M, Bao QL, Loh KP (2012) Electrocatalytically active graphene–porphyrin MOF composite for oxygen reduction reaction. J Am Chem Soc 134:6707–6713
36. Sadeghi N, Sharifnia S, Sheikh Arabi M (2016) A porphyrin-based metal organic framework for high rate photoreduction of CO_2 to CH_4 in gas phase J CO_2 Util. 16: 450–457
37. Wang X, Wang QX, Wang QH, Gao F, Yang YZ, Guo HX (2014) Highly dispersible and stable copper terephthalate metal−organic framework−graphene oxide nanocomposite for an electrochemical sensing application. ACS Appl Mater Interfaces 6:11573–11580
38. Ang HX, Hong L (2017) Polycationic polymer-regulated assembling of 2D MOF nanosheets for high-performance nanofiltration. ACS Appl Mater Interfaces 9:28079–28088
39. Liu M, Xie K, Nothling MD, Gurr PA, Tan SSL, Fu Q, Webley PA, Qiao GG (2018) Ultrathin metal-organic framework nanosheets as a gutter layer for flexible composite gas separation membranes. ACS Nano 12:11591–11599